ACS Catalysis

Research Article

pubs.acs.org/acscatalysis

Tin and Silicon Binary Oxide on the Carbon Support of a Pt Electrocatalyst with Enhanced Activity and Durability

Fan Luo, Shijun Liao,* Dai Dang, Yan Zheng, Dongwei Xu, Haoxiong Nan, Ting Shu, and Zhiyong Fu

The Key Laboratory of Fuel Cell Technology of Guangdong Province & The Key Laboratory of New Energy Technology of Guangdong Universities, School of Chemistry and Chemical Engineering, South China University of Technology, Guangzhou 510641, People's Republic of China

Supporting Information

ABSTRACT: Poor durability is one of the two major problems hindering the commercialization of proton exchange membrane fuel cells, due to Pt nanoparticle aggregation in the electrocatalyst and corrosion of its carbon support. In this paper, we report a Pt electrocatalyst in which carbon black decorated with a tin and silicon binary oxide layer was used as the support, with SnO_2 as a promoter and SiO_2 as a stabilizer. Transmission electron microscopy revealed that the binary oxide formed a thin layer on the surface of the carbon support particles. The catalyst exhibited significantly enhanced performance toward the oxygen reduction reaction (ORR): at 0.9 V (vs RHE), the ORR current density was ~1.5 times higher than that of a commercial JM Pt/C catalyst with the same Pt loading. Furthermore, it showed excellent durability, again better than that of JM Pt/C: after 8000 cyclic voltammetry cycles in 0.5 M H_2SO_4 solution, the electrochemically active surface area was almost unchanged and the ORR half-wave potential shifted by only 10 mV. We attribute the catalyst's high activity and durability to the binary oxide coating the surface of the carbon nanoparticles. We suggest it may play two roles: (1) promoted by tin oxide and thereby enhancing the catalytic activity and (2) preventing the Pt nanoparticles from aggregating and carbon support from corrosion. The high ORR performance and excellent stability of this catalyst make it promising for use in practical fuel cell applications.

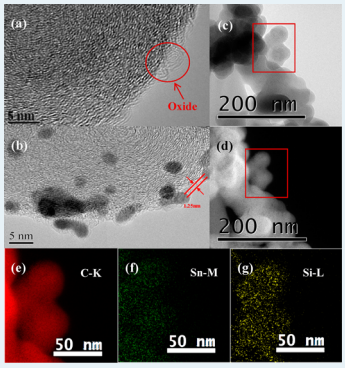

KEYWORDS: *binary oxide, decorate, carbon support, Pt electrocatalyst, ORR, durability*

1. INTRODUCTION

Proton exchange membrane fuel cells (PEMFCs) have drawn significant attention as highly efficient, environmentally benign power sources with a wide range of potential applications in many areas, including transportation, military technology, and portable energy storage.[1,2] However, two major interrelated challenges still prevent their widespread use: high cost and poor durability, both mainly caused by limitations in fuel cell catalysts.[3−7]

Many researchers have reported that the poor durability of PEMFCs generally results from Pt nanoparticle aggregation, which is closely related to the support materials used in Pt-based catalysts. Currently, fuel cell technology uses carbon black as the primary catalyst support, due to its high electrical conductivity, acceptable chemical stability, and low cost.[8−11] However, carbon black suffers from two important limitations. First, carbon support corrosion has been identified as one of the main reasons for Pt surface area loss and reduced fuel cell durability during operation.[12,13] Second, the predominance of weak interactions between the carbon support and the catalytic metal nanoparticles (NPs) leads to sintering of those NPs and a consequent decrease in the active surface area during long-term operation.[14] Researchers worldwide have put significant effort into overcoming these problems. Some, for example, have tried functionalizing the carbon support with other materials,[15−20] or even replacing it with oxide supports.[21−31]

According to the literature, oxide modification not only can promote the performance of Pt catalysts toward methanol oxidation at the anode[32−35] and oxygen reduction at the cathode[36,37] but also can significantly enhance catalyst stability and durability by preventing Pt NP aggregation and carbon support corrosion.[38] Some researchers have reported that tin dioxide (SnO_2) is an effective additive for modifying a carbon support or carbon-supported Pt catalysts.[39−42] However, SnO_2 suffers from poor stability at potentials relevant to the ORR because SnO_2 can dissolve under acidic conditions.

To overcome this drawback of tin oxide, in the present study we used a binary oxide of tin and silicon to modify the carbon support. Using a novel process, we prepared a modified carbon support in which the carbon support was covered with a thin layer of $Sn_{0.3}Si_{0.7}O_x$ oxide, the silicon oxide functioning to stabilize the tin oxide. The oxide layer physically deposited on the carbon surface or attached with a weak chemical bond, which protected the carbon structure from destruction. The resulting Pt catalyst, supported on binary oxide modified carbon black (XC72R), exhibited not only significantly enhanced activity toward methanol oxidation and oxygen

Received: May 23, 2014
Revised: December 2, 2014
Published: December 3, 2014

DOI: 10.1021/cs501429g
ACS Catal. 2015, 5, 2242−2249

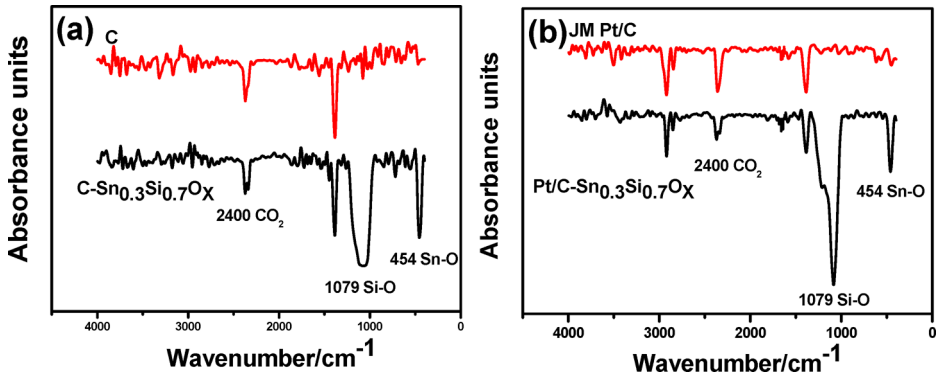

Figure 1. FTIR spectra: (a) carbon black and C-$Sn_{0.3}Si_{0.7}O_x$; (b) JM Pt/C and Pt/C-$Sn_{0.3}Si_{0.7}O_x$.

reduction but also excellent stability, demonstrating that the tin oxide was effectively stabilized by the addition of silicon oxide.

2. EXPERIMENTAL SECTION

2.1. Decoration of Carbon Support. The typical preparation procedures were as follows. First, 100 mg of pristine carbon black (Vulcan XC72R) was dispersed in 10 mL of an ethanol solution containing 8 mg of tin tetrachloride ($SnCl_4$) and 20 μL of tetraethyl silicate (TEOS). The mixture was then sonicated for 1 h to achieve high dispersion, after which the solvent was evaporated, the $SnCl_4$ and TEOS were slowly hydrolyzed, and a binary oxide thin film formed over the surface of the carbon black particles. This coated carbon black was then calcined under an Ar flow at 300 °C for 3 h. We denote the resulting binary oxide functionalized/covered carbon black as C-$Sn_{0.3}Si_{0.7}O_x$ (the calculated oxide content was ca. 10%). For comparison, SnO_2-decorated carbon black (denoted as C-SnO_2) and SiO_2-decorated carbon black (denoted as C-SiO_2) were prepared using $SnCl_4$ and TEOS as the respective precursors.

2.3. Catalyst Preparation. The supported platinum catalysts in this work were prepared using a colloidal method reported previously by our group.[43] First, 120 mg of hexachloroplatinic acid and 300 mg of sodium citrate were dissolved in a mixture of 9 mL of acetone and 9 mL of ethylene glycol (EG), and then the mixture was stirred for 0.5 h. After the citrate had entirely dissolved, 100 mg of functionalized carbon black (C-$Sn_{0.3}Si_{0.7}O_x$, C-SnO_2, or C-SiO_2) was added; the pH value of the system was then adjusted to >10 by dropwise addition of 5 wt % KOH/EG solution with vigorous stirring. Next, the mixture was transferred into an autoclave with a Teflon liner and underwent reaction at 120 °C for 6 h, followed by filtering, washing with deionized water, and drying under vacuum at 60 °C overnight. The theoretical Pt loading is 20 wt %.

2.3. Materials Characterization. The existence of Nafion was detected by Fourier transform infrared spectroscopy (FTIR) using a Tensor 27 (Bruker, Germany) spectrometer. Transmission electron microscopy (TEM) was performed using a JEOL 2010 with an acceleration voltage of 200 keV. An X-ray diffractometer (Tongda, TD-3500, People's Republic of China) was used to identify the crystalline structure and measure the average crystallite size of the Pt NPs. Contact angles were measured using an OCA 40 video-based optical contact angle meter (Dataphysics, Germany).

2.4. Electrochemical Measurements. Electrochemical measurements were carried out on an electrochemical workstation (Ivium, The Netherlands) at room temperature using a standard three-electrode electrochemical cell. A platinum wire and an Ag/AgCl (3 M KCl) electrode were used as the counter and reference electrodes, respectively. The potential of the Ag/AgCl (3 M KCl) was calibrated with a RHE reference electrode (in 0.1 M KOH, E(RHE) = E(Ag/AgCl) + 0.982 V; in 0.1 M $HClO_4$, E(RHE) = E(Ag/AgCl) + 0.288 V). The typical preparation process for the working electrode was as follows: 5 mg of the catalyst was dispersed ultrasonically in 1 mL of Nafion/ethanol (0.25 wt % Nafion) for 0.5 h, and then 5 μL of this catalyst dispersion was pipetted and spread on a glassy-carbon electrode (5 mm inner diameter), followed by drying under an infrared bulb. All potentials in the present study are quoted versus an RHE electrode.

The electrochemically active surface area (ECSA) of the catalyst was measured in a nitrogen-saturated 0.5 M H_2SO_4 solution at a scan rate of 50 mV s^{-1}, and the catalyst's activity for the methanol oxidation reaction was measured in a nitrogen-saturated 0.5 M H_2SO_4 + 0.5 M CH_3OH solution at a scan rate of 50 mV s^{-1}. ORR tests were conducted in an oxygen-saturated 0.1 M $HClO_4$ solution at a scan rate of 10 mV s^{-1}. All tests were conducted at room temperature.

3. RESULTS AND DISCUSSION

3.1. Characterization. Figure 1 presents the FTIR spectra of the carbon support and catalysts. As Figure 1a shows, C-

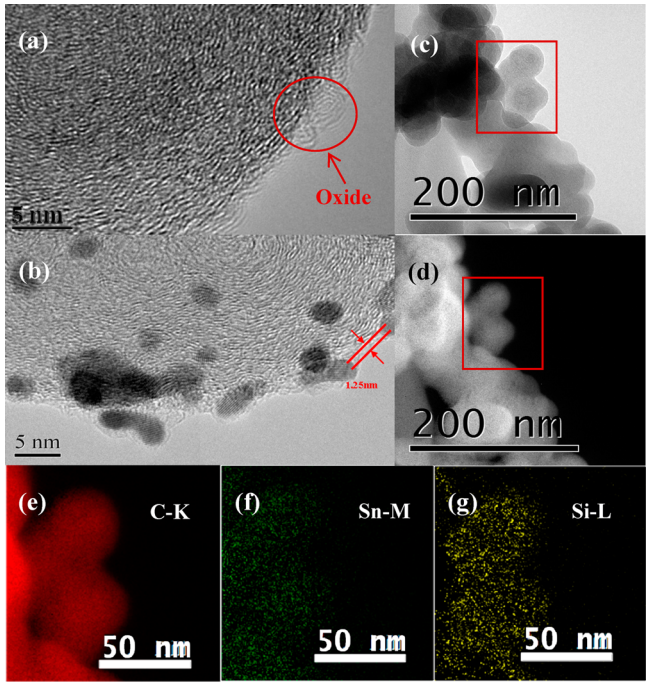

Figure 2. HRTEM images of (a) C-$Sn_{0.3}Si_{0.7}O_x$ and (b) Pt/C-$Sn_{0.3}Si_{0.7}O_x$. (c) BF and (d) ADF STEM images of C-$Sn_{0.3}Si_{0.7}O_x$ nanoparticles. Corresponding EELS maps of (e) C-K, (f) Sn-M, and (g) Si-L, respectively.

$Sn_{0.3}Si_{0.7}O_x$ displays a very strong absorption peak at 1063 cm^{-1}, which is attributable to the vibration of the Si−O band.[44] The peak at 454 cm^{-1} can be assigned to the vibration of the Sn−O band.[45] Figure 1b shows that the oxide remains on the commercial (Johnson Matthey, JM) Pt/C after the preparation

DOI: 10.1021/cs501429g
ACS Catal. 2015, 5, 2242−2249

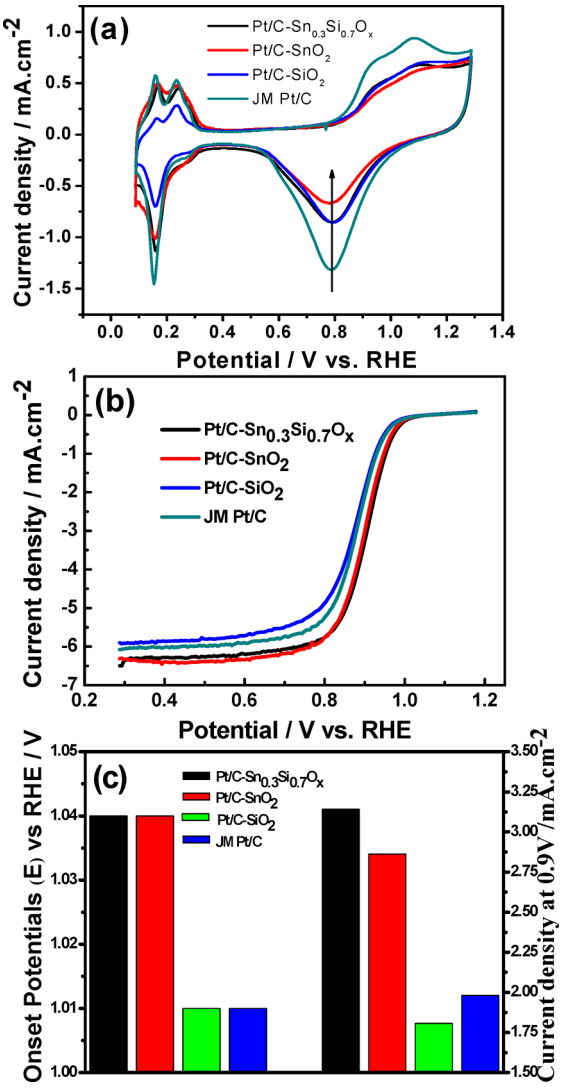

Figure 3. (a) Cyclic voltammograms of Pt/C-$Sn_{0.3}Si_{0.7}O_x$, Pt/C-SnO_2, Pt/C-SiO_2, and JM Pt/C catalysts in N_2-saturated 0.5 M H_2SO_4 electrolyte at room temperature with a sweep rate of 50 mV s^{-1}. (b) ORR polarization curves of Pt/C-$Sn_{0.3}Si_{0.7}O_x$, Pt/C-SnO_2, Pt/C-SiO_2, and JM Pt/C catalysts in O_2-saturated 0.1 M $HClO_4$ solution at a rotation rate of 1600 rpm. (c) Histogram of onset potentials (E, vs RHE) and ORR current densities at 0.9 V of Pt/C-$Sn_{0.3}Si_{0.7}O_x$, Pt/C-SnO_2, Pt/C-SiO_2, and JM Pt/C catalysts.

and washing processes. In summary, the FTIR results confirm the existence of SnO_2 and SiO_2 together on the catalyst surface, showing that the combination did not wash off during the colloidal procedures required for the deposition of Pt NPs. The XRD patterns given in section 3.3 also confirm the binary oxide's presence in the final catalysts.

Figure 2a,b presents typical high-resolution TEM (HRTEM) images of the oxide-decorated carbon C-$Sn_{0.3}Si_{0.7}O_x$ and Pt/C-$Sn_{0.3}Si_{0.7}O_x$ catalyst. From the images, we can see the coverage of amorphous oxide on the surface of the carbon support particles and the Pt/C-$Sn_{0.3}Si_{0.7}O_x$ catalyst. The average thickness of the covering layer is ca. 1.2 nm. From these findings combined with the results presented in Figure 1, we guess that SnO_2 and SiO_2 were combined and present on the catalyst's surface. To further confirm our speculation, the chemical distribution of C-$Sn_{0.3}Si_{0.7}O_x$ nanoparticles was examined using a scanning transmission electron microscope (STEM) equipped (FEI tecnai G2 F30 (300 kV)) with an Enfina electron energy loss spectrometer (EELS). Figure 2c,d shows both bright-field (BF) and annular dark-field (ADF) STEM images simultaneously acquired prior to EELS map acquisition. The component elements of the marked area in Figure 2c,d were analyzed using energy-dispersive X-ray analysis (EDX) (Figure S1, Supporting Information). The EDX analysis shows a strong C peak and reasonably strong Si and Sn peaks from C-$Sn_{0.3}Si_{0.7}O_x$. The Cu signal may result from the lacey support films used. Figure 2e–g shows the EELS distribution maps of C, Sn, and Si, which reveal clearly that Sn and Si were highly and uniformly distributed on the surface of the C support.

3.2. Performance Enhancement. Figure 3a shows cyclic voltammograms (CVs) of Pt/C catalysts with different oxide thin films in a N_2-purged 0.5 M H_2SO_4 solution at a scan rate of 50 mV s^{-1}. We have measured the Pt content of each catalyst by atomic adsorption spectroscopy (AAS). The Pt contents of all catalysts were similar, as were the Pt contents on the glassy-carbon electrodes. It can be seen that the hydrogen adsorption peaks of the Pt/C-$Sn_{0.3}Si_{0.7}O_x$ and Pt/C-SiO_2 catalysts were significantly smaller than those of the Pt catalyst. Other researchers have reported similar results.[46,47] They suggested that hydrogen adsorption on Pt decreased because either some of the Pt active sites for hydrogen adsorption were blocked or the electronic properties of Pt were significantly changed by the addition of other elements.

In comparison with the case for the JM Pt/C catalyst, the oxidation of Pt and adsorption/desorption of hydrogen of the catalyst with oxide/binary oxide loaded carbon as support are depressed significantly (Figure 3a), the Pt/C-SnO_2 catalyst exhibits the smallest Pt oxidation/reduction peaks, and the Pt/C-SiO_2 catalyst exhibits the smallest hydrogen adsorption/desorption peaks. Clearly, the decoration of SiO_2 may inhibit the active surface area, but the decoration with SnO_2 or $Sn_{0.3}Si_{0.7}O_x$ binary oxide just slightly affects the active surface area and strongly affects the oxidation/reduction of the Pt active component. Thus, we believe that there should be an interaction between the Pt NPs and SnO_2, which may prevent the Pt NPs from surface oxidation to form Pt–O bonds. Further, we suggest that the interaction between Pt and SnO_2 may be one of the possible reasons for the ORR performance improvements of the catalyst with binary oxide decorated carbon as support.

As shown in Figure 3b,c, the ORR performance of the catalyst with the binary oxide thin film was significantly improved by this addition. In comparison with JM Pt/C and with Pt/C-SiO_2, the onset potential of Pt/C-$Sn_{0.3}Si_{0.7}O_x$ shifted by over 30 mV, and the current density at 0.9 V (vs RHE) increased by over 50%.

It is interesting that, if only silicon oxide was coated on the carbon support, the ORR performance of Pt/C-SiO_2 was not at all enhanced and in fact decreased slightly. However, Pt/C-SnO_2—with only SnO_2 coating the carbon support—exhibited excellent performance enhancement, inferior only to that of Pt/C-$Sn_{0.3}Si_{0.7}O_x$. It is clear that adding just SnO_2 can enhance the Pt-based catalyst's performance, but the coaddition of SiO_2 augments the enhancement.

3.3. Effect of Calcining Temperature. We believed that a binary oxide covered carbon support calcined at an appropriate temperature would strengthen the bonding/combination of the binary oxide with the carbon support, which would in turn improve the stability of the binary oxide in the catalyst.[48−50] On

DOI: 10.1021/cs501429g
ACS Catal. 2015, 5, 2242−2249

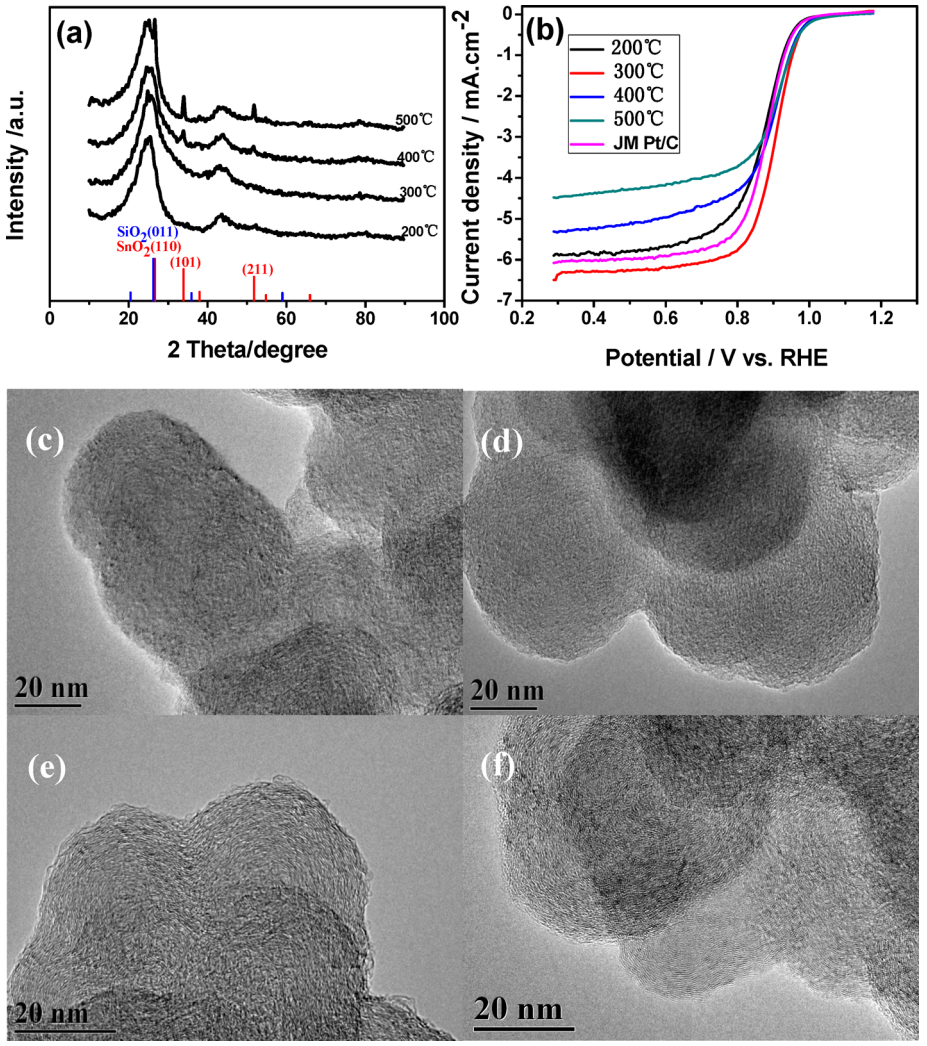

Figure 4. (a) XRD patterns of C-$Sn_{0.3}Si_{0.7}O_x$ without support of Pt calcined at different temperatures for 3 h. (b) ORR polarization curves of Pt/C-$Sn_{0.3}Si_{0.7}O_x$ catalysts calcined at different temperatures in 0.5 M H_2SO_4 solution saturated with pure oxygen, at a scanning rate of 10 mV s^{-1} and a rotation speed of 1600 rpm. TEM images of (c) XC-72R, and of C-$Sn_{0.3}Si_{0.7}O_x$ calcined for 3 h at (d) 200 °C, (e) 300 °C, and (f) 400 °C.

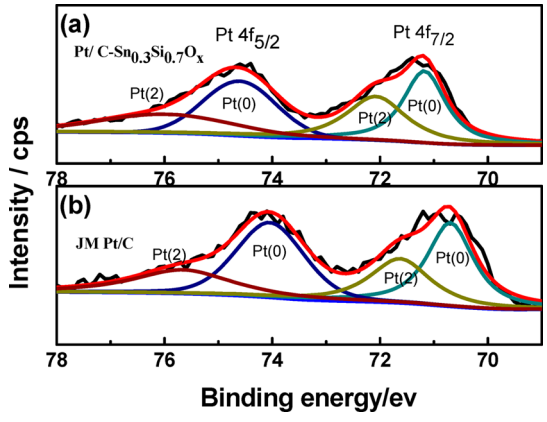

Figure 5. XPS spectra of Pt 4f: (a) Pt/C-$Sn_{0.3}Si_{0.7}O_x$; (b) JM Pt/C.

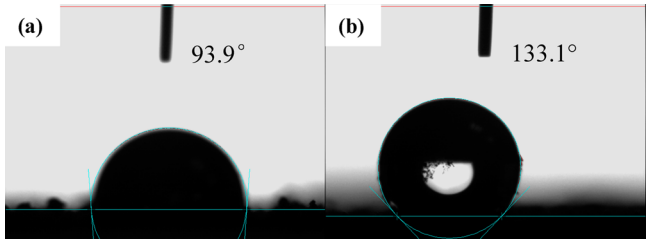

Figure 6. Contact angle images: (a) Pt/C-$Sn_{0.3}Si_{0.7}O_x$; (b) JM Pt/C.

the basis of this idea, we investigated the effect of calcining temperature on the catalysts' structure and performance. Figure 4a presents the XRD patterns of C-$Sn_{0.3}Si_{0.7}O_x$ support calcined at different temperatures for 3 h in each case. When the calcining temperature is below 400 °C, no obvious oxide diffraction peaks can be observed. At 400 °C, oxide diffraction peaks appear, implying that below 400 °C the binary oxide exists on the carbon support mainly in an amorphous form; this is confirmed by the HRTEM images shown in Figure 4c–f.

Figure 4b shows the ORR performance of Pt/C-$Sn_{0.3}Si_{0.7}O_x$ catalysts when the support was calcined at different temperatures. The results indicate that the catalyst whose support was calcined at 300 °C exhibited the best ORR activity. The catalyst whose support was calcined at 200 °C exhibited much lower ORR performance, similar to that of JM Pt/C, which may have been due to the weak bonding between the oxide and the carbon support at this low temperature. Conversely, when the calcining temperature was too high, the oxides aggregated into

DOI: 10.1021/cs501429g
ACS Catal. 2015, 5, 2242–2249

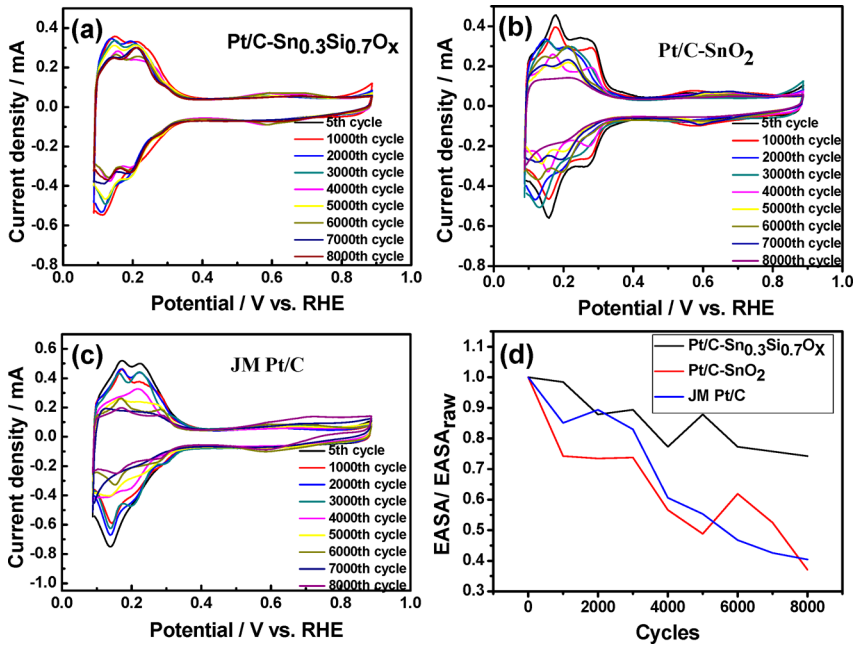

Figure 7. CV curves of electrodes made from (a) Pt/C-$Sn_{0.3}Si_{0.7}O_x$, (b) Pt/C-SnO_2, and (c) JM Pt/C catalysts for different numbers of CV cycles in N_2-saturated 0.5 M H_2SO_4 solution at a scanning rate of 100 mV s^{-1}. (d) Comparison of ECSA loss for different catalysts. $ECSA_{raw}$ is the initial ECSA of the corresponding catalyst.

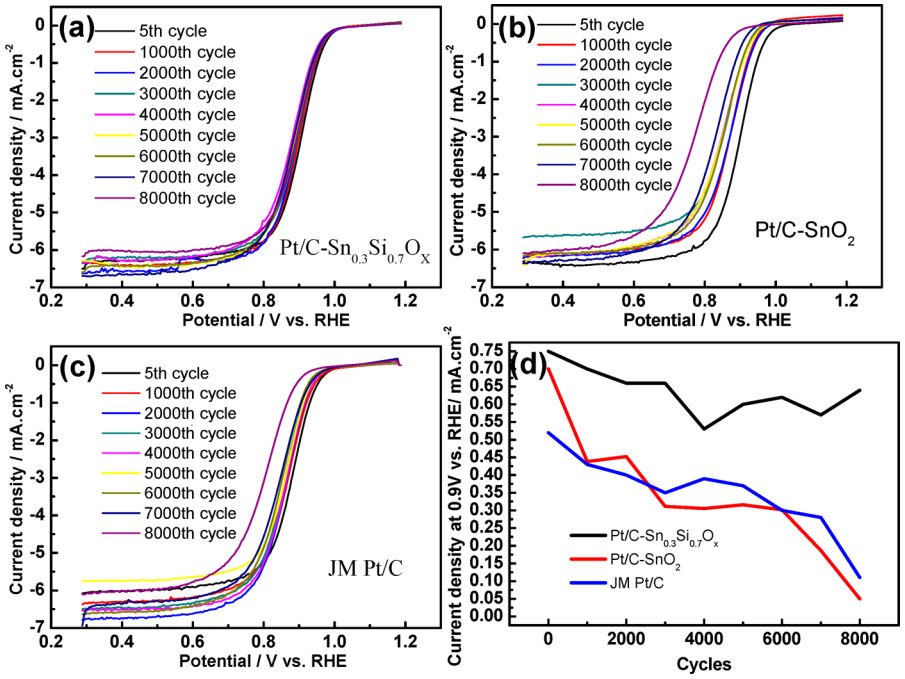

Figure 8. ORR polarization curves of (a) Pt/C-$Sn_{0.3}Si_{0.7}O_X$, (b) Pt/C-SnO_2, and (c) JM Pt/C catalysts for different numbers of CV cycles in O_2-saturated 0.1 M $HClO_4$ solution at a scanning rate of 10 mV s^{-1}. (d) ORR current density at 0.9 V vs RHE of catalysts after potential cycling.

large particles, the limit current density reduced by the effect of active sites.

3.3. Interactions and Mechanism. Figure 5 shows the XPS spectra of Pt 4f in the Pt/C-$Sn_{0.3}Si_{0.7}O_x$ and JM Pt/C catalysts. For Pt/C-$Sn_{0.3}Si_{0.7}O_x$, the respective binding energies of Pt $4f_{5/2}$ and Pt $4f_{7/2}$ are 71.2 and 74.6 eV, in comparison to 70.6 and 74.0 eV for JM Pt/C. Both Pt/C-$Sn_{0.3}Si_{0.7}O_2$ binding energies are 0.6 eV higher than the values for Pt/C. Generally, these shifts can be attributed to electron delocalization between the d orbitals of Pt and the $Sn_{0.3}Si_{0.7}O_x$; this causes partial ionization of Pt, due to electron transfer from Pt to $Sn_{0.3}Si_{0.7}O_x$, and Pt back-donates electrons to the adjacent Sn_{pz} orbitals.[51,52] The electron delocalization between the Pt NPs and Sn alters the electronic structure of the Pt NPs, making it difficult for the Pt NPs to lose/release additional electrons (i.e., to be oxidized). Prevention of the dissolution of Pt via the formation of Pt−O bonds is beneficial. This assertion can be discerned in the CVs of the catalysts in Figure 3a. The JM Pt/C catalyst showed a Pt oxide reduction peak at 0.8 V vs RHE, higher than that for other catalysts, which means that the addition of oxide prevents

DOI: 10.1021/cs501429g
ACS Catal. 2015, 5, 2242−2249

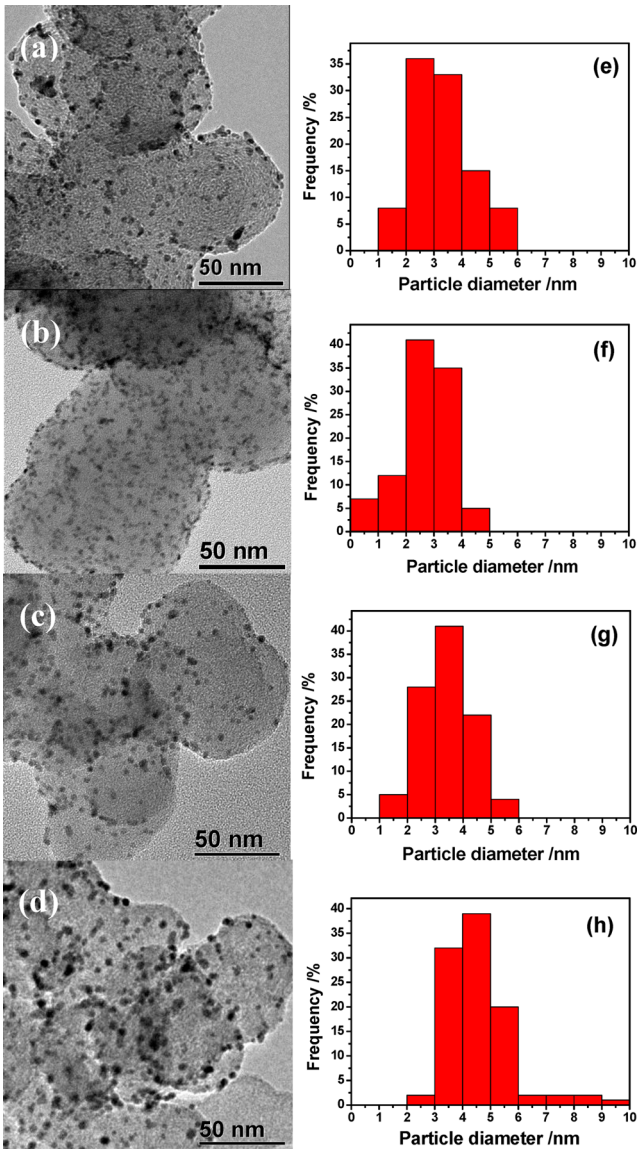

Figure 9. TEM images of (a) fresh Pt/C-$Sn_{0.3}Si_{0.7}O_x$ catalyst, (b) fresh JM Pt/C catalyst, and (c) aged Pt/C-$Sn_{0.3}Si_{0.7}O_x$ catalyst after 8000 CV cycles and (d) aged JM Pt/C catalyst after 8000 CV cycles. Pt particle-distribution histograms of (e) fresh Pt/C-$Sn_{0.3}Si_{0.7}O_x$ catalyst, (f) fresh JM Pt/C catalyst, (g) aged Pt/C-$Sn_{0.3}Si_{0.7}O_x$ catalyst after 8000 CV cycles, and (h) aged JM Pt/C catalyst after 8000 CV cycles.

the oxidation of Pt (or formation of Pt-O). We also analyzed the Si 2p and Sn 3d orbitals. However, the amounts of Sn and Si were sufficiently low that the peaks in the XPS spectrum were not obvious and hence are not discussed here.

On one hand, the electron delocalization between the Pt NPs and Sn alters the electronic structure of the Pt NPs, making it difficult for the Pt NPs to lose/release additional electrons. On the other hand, the interaction between Pt and $Sn_{0.3}Si_{0.7}O_x$ prevents the Pt NPs from being oxidized,[53] which enhances the catalyst's stability.

We believe that the addition of oxides may benefit from the adsorption and reduction of oxygen by modifying the surface of the carbon support. To further reveal and understand the enhancement mechanism in Pt/C-$Sn_{0.3}Si_{0.7}O_x$ catalyst, we assessed the wetting properties of Pt/C-$Sn_{0.3}Si_{0.7}O_x$ and JM Pt/C using contact angle measurements. Figure 6 shows the contact angles of Pt/C-$Sn_{0.3}Si_{0.7}O_x$ and JM Pt/C. Clearly, with the addition of oxides, the contact angle decreases significantly. These results reveal that adding oxides can improve the hydrophilicity of the catalyst, which may make it easier for adsorption and reduction to occur on its surface.

3.4. Stability of the Catalyst. Generally, the stability of a fuel cell catalyst can be determined from attenuation of the ECSA after long-term cyclic voltammetry.[53] Figure 7 displays the long-term (8000 cycles) CV results for Pt/C-$Sn_{0.3}Si_{0.7}O_x$, Pt/C-SnO_2, and JM Pt/C (Figure 7a–c, respectively) in nitrogen-saturated 0.5 M H_2SO_4 solution, as well as the ECSA attenuation results for each catalyst. It can be seen that the Pt/C-$Sn_{0.3}Si_{0.7}O_X$ catalyst shows amazing stability; after 8000 CV cycles, almost no recordable ECSA loss can be observed. However, the ECSA attenuation in the cases of JM Pt/C and Pt/C-SnO_2 is up to 60%, indicating that a catalyst support composed of carbon black decorated with $Sn_{0.3}Si_{0.7}O_x$ thin film greatly enhances the stability of a Pt catalyst.

To further investigate the stability of our oxide-decorated catalyst, we conducted long-term ORR tests with Pt/C-$Sn_{0.3}Si_{0.7}O_X$, Pt/C-SnO_2, and JM Pt/C and found that the stability of Pt/C-$Sn_{0.3}Si_{0.7}O_X$ was far superior. The current density of Pt/C-$Sn_{0.3}Si_{0.7}O_X$ at 0.9 V (vs RHE) decreased by only 14.7% after 8000 CV cycles in 0.5 M H_2SO_4 solution (Figure 8). In contrast, the current densities of Pt/C-SnO_2 and Pt/C decreased by 92.9% and 52.5%, respectively. Interestingly, at the beginning, the ORR performance of Pt/C-SnO_2 was almost that of Pt/C-$Sn_{0.3}Si_{0.7}O_x$, but after 1000 cycles, it was close to that of JM Pt/C. This demonstrated the significance of SiO_2 stably coexisting with SnO_2 on the surface of the catalyst in acid solution; without this coexistence, catalyst performance was lost.

Using HRTEM to analyze the catalysts before and after long-term ORR testing, we obtained some interesting results, as shown in Figure 9. In the case of JM Pt/C, the average particle size of the Pt NPs increased from ca. 3 to 4.5 nm, with a broader size distribution after 8000 CV cycles in 0.5 M H_2SO_4 solution, indicating that strong ripening or aggregation of the Pt NPs occurred during CV cycling. In contrast, the average particle size of the Pt NPs in Pt/C-$Sn_{0.3}Si_{0.7}O_x$ remained almost unchanged, confirming that Pt/C-$Sn_{0.3}Si_{0.7}O_x$ is more electrochemically stable than JM Pt/C.

Regarding the mechanism of this far superior stability, we suggest three factors. (1) The oxides have a restrictive effect on the Pt NPs; as shown in Figure 9a, aggregation of the Pt NPs is inhibited because the NPs are separated by the oxides. (2) Strong interactions between the Pt NPs and the oxides may also prevent Pt NPs from aggregating. (3) By covering the carbon black, the oxides may protect the support from electrochemical corrosion, which is recognized as one of the most important factors leading to the aggregation of Pt NPs in fuel cell catalysts. The use of differential electrochemical mass spectroscopy (DEMS) to investigate the electrochemical oxidation of carbon reveals that, in the presence of Pt, CO_{surf} is formed on the carbon at $E > 0.3$ V (RHE) and is then oxidized to CO_2 at potentials between 0.6 and 0.8 V (RHE).[54] Electrochemical corrosion of the carbon support causes agglomeration and sintering of the Pt catalyst particles, which decreases the catalyst's ECSA. Carbon corrosion also leads to electrically isolated Pt particles that are detached from the support. These effects result in rapid degradation of the Pt catalyst and thus affect its performance.[40] In the present study, the carbon black decorated with $Sn_{0.3}Si_{0.7}O_x$ was more robust

DOI: 10.1021/cs501429g
ACS Catal. 2015, 5, 2242–2249

because the oxide layer protected the carbon support from corrosion.

CONCLUSION

In conclusion, we are able to report a Pt electrocatalyst with significantly enhanced performance and ultrahigh stability, formed by using silicon and tin binary oxide to decorate the carbon black support; SnO_2 is employed as a promoter and SiO_2 as a stabilizer. TEM reveals that the binary oxide forms a thin layer over the carbon support. We also demonstrate that the activity of the catalyst is significantly enhanced by this decorated carbon black support: for the ORR, the catalyst's current density at 0.9 V (vs RHE) is ~1.5 times higher than that of commercial Pt/C with the same Pt loading. Furthermore, the catalyst with the decorated carbon support exhibits much better stability/durability than commercial Pt/C. After 8000 CV cycles in 0.5 M H_2SO_4 solution, the electrochemically active area is almost unchanged and the ORR half-wave potential shifts by only 10 mV. We attribute the catalyst's high activity and stability/durability to the binary oxide that coats the surface of the carbon support. This binary oxide may have two functions: (1) promotion by tin oxide and (2) prevention of carbon black corrosion and Pt nanoparticle aggregation. We found that the coexistence of silicon oxide and tin oxide on the surface of the carbon support is crucial for the catalyst's ultrahigh stability because silicon oxide prevents the dissolution of tin oxide. The high ORR performance and excellent stability of the catalyst with this decorated carbon support make it a promising electrocatalyst for practical fuel cell applications.

ASSOCIATED CONTENT

Supporting Information

The following file is available free of charge on the ACS Publications website at DOI: 10.1021/cs501429g.

EDX analysis of C-$Sn_{0.3}Si_{0.7}O_x$ (PDF)

AUTHOR INFORMATION

Corresponding Author

*E-mail for S.L.: chsjliao@scut.edu.cn.

Notes

The authors declare no competing financial interest.

ACKNOWLEDGMENTS

This work has been supported by the National Foundation of China (NFC Project No. 21276098), the Natural Scientific Foundation of Guangdong Province, People's Republic of China (NSFGC Project No. S2012020011061), and the Science and Technology 863 Foundation (STF Project No. 2012AA053402).

REFERENCES

(1) Di Noto, V.; Negro, E. *Fuel Cells* **2010**, *10*, 234−244.
(2) Mehta, V.; Cooper, J. S. *J. Power Sources* **2003**, *114*, 32−53.
(3) Borup, R.; Meyers, J.; Pivovar, B.; Kim, Y. S.; Mukundan, R. *Chem. Rev.* **2007**, *107*, 3904−3951.
(4) Lee, K.-S.; Jeon, T.-Y.; Yoo, S. J.; Park, I.-S.; Cho, Y.-H.; Kang, S. H.; Choi, K. H.; Sung, Y.-E. *Appl. Catal. B: Environ.* **2011**, *102*, 334−342.
(5) Ding, K.; Liu, L.; Cao, Y.; Yan, X.; Wei, H.; Guo, Z. *Int. J. Hydrogen Energy* **2014**, *39*, 7326−7337.
(6) Ding, K.; Wang, Y.; Yang, H.; Zheng, C.; YanliCao; Wei, H.; Wang, Y.; Guo, Z. *Electrochim. Acta* **2013**, *100*, 147−156.
(7) Ding, K.; Jia, H.; Wei, S.; Guo, Z. *Ind. Eng. Chem. Res.* **2011**, *50*, 7077−7082.
(8) Fang, B.; Chaudhari, N. K.; Kim, M.-S.; Kim, J. H.; Yu, J.-S. *J. Am. Chem. Soc.* **2009**, *131*, 15330−15338.
(9) Antolini, E. *Appl. Catal. B: Environ.* **2009**, *88*, 1−24.
(10) Dicks, A. L. *J. Power Sources* **2006**, *156*, 128−141.
(11) Zhao, D.; Xu, B. Q. *Angew. Chem.* **2006**, *45*, 4955−4959.
(12) Ombaka, L. M.; Ndungu, P.; Nyamori, V. O. *Catal. Today* **2013**, *217*, 65−75.
(13) Shao, Y.; Yin, G.; Gao, Y. *J. Power Sources* **2007**, *171*, 558−566.
(14) Subban, C. V.; Zhou, Q.; Hu, A.; Moylan, T. E.; Wagner, F. T.; DiSalvo, F. J. *J. Am. Chem. Soc.* **2010**, *132*, 17531−17536.
(15) Wang, S.; Wang, X.; Jiang, S. P. *Langmuir* **2008**, *24*, 10505−10512.
(16) Lu, J. D.; Yang, M.-C. *J. Power Sources* **2011**, *196*, 7450−7457.
(17) Wang, S.; Yu, D.; Dai, L.; Chang, D. W.; Baek, J.-B. *ACS Nano* **2011**, *5*, 6202−6209.
(18) Wang, S.; Jiang, S. P.; Wang, X. *Nanotechnology* **2008**, *19*, 265601.
(19) Selvaraj, V.; Alagar, M. *Electrochim. Commun.* **2007**, *9*, 1145−1153.
(20) Wang, S.; Yu, D.; Dai, L. *J. Am. Chem. Soc.* **2011**, *133*, 5182−5185.
(21) Lin, Y.-H.; Hsueh, Y.-C.; Lee, P.-S.; Wang, C.-C.; Wu, J. M.; Perng, T.-P.; Shih, H. C. *J. Mater. Chem.* **2011**, *21*, 10552−10558.
(22) Chen, Y.; Wang, J.; Meng, X.; Zhong, Y.; Li, R.; Sun, X.; Ye, S.; Knights, S. *Int. J. Hydrogen Energy* **2011**, *36*, 11085−11092.
(23) Silva, J. C. M.; De Souza, R. F. B.; Parreira, L. S.; Neto, E. T.; Calegaro, M. L.; Santos, M. C. *Appl. Catal. B: Environ.* **2010**, *99*, 265−271.
(24) Wang, L.; Yamauchi, Y. *J. Am. Chem. Soc.* **2010**, *132*, 13636−13638.
(25) Kowal, A.; Gojković, S. L.; Lee, K. S.; Olszewski, P.; Sung, Y. E. *Electrochem. Commun.* **2009**, *11*, 724−727.
(26) Lee, K.; Park, I.; Cho, Y.; Jung, D.; Jung, N.; Park, H.; Sung, Y. *J. Catal.* **2008**, *258*, 143−152.
(27) Ahn, H.-J.; Choi, H.-C.; Park, K.-W.; Kim, S.-B.; Sung, Y.-E. *J. Phys. Chem. B* **2004**, *108*, 9815−9820.
(28) Baker, L.; Cavanagh, A. S.; Seghete, D.; George, S. M.; Mackus, A. J. M.; Kessels, W. M. M.; Liu, Z. Y.; Wagner, F. T. *J. Appl. Phys.* **2011**, *109*, 084333.
(29) Lee, H.-B.-R.; Bent, S. F. *Chem. Mater.* **2012**, *24*, 279−286.
(30) Chen, C.-S.; Pan, F.-M. *Appl. Catal. B: Environ.* **2009**, *91*, 663−669.
(31) Shanmugam, S.; Gedanken, A. *Small* **2007**, *3*, 1189−1193.
(32) Nouralishahi, A.; Khodadadi, A. A.; Rashidi, A. M.; Mortazavi, Y. *J. Colloid Interface Sci.* **2013**, *393*, 291−299.
(33) Ye, J.; Liu, J.; Zou, Z.; Gu, J.; Yu, T. *J. Power Sources* **2010**, *195*, 2633−2637.
(34) Wu, F.; Liu, Y.; Wu, C. *Journal of Wuhan University of Technology-Mater. Sci. Ed.* **2011**, *26*, 377−383.
(35) Wu, F.; Liu, Y.; Wu, C. *Rare Metals* **2010**, *29*, 255−260.
(36) Ma, C.; Jin, Y.; Shi, M.; Chu, Y.; Xu, Y.; Jia, W.; Yuan, Q.; Chen, J.; Chen, D.; Chen, S. *J. Electro. Soc.* **2013**, *161*, F246−F251.
(37) Zhang, N.; Zhang, S.; Du, C.; Wang, Z.; Shao, Y.; Kong, F.; Lin, Y.; Yin, G. *Electrochim. Acta* **2014**, *117*, 413−419.
(38) Zhu, T.; Du, C.; Liu, C.; Yin, G.; Shi, P. *Appl. Surf. Sci.* **2011**, *257*, 2371−2376.
(39) Ho, V. T.; Pan, C. J.; Rick, J.; Su, W. N.; Hwang, B. J. *J. Am. Chem. Soc.* **2011**, *133*, 11716−11724.
(40) Huang, S.-Y.; Ganesan, P.; Park, S.; Popov, B. N. *J. Am. Chem. Soc.* **2009**, *131*, 13898.
(41) Shao, Y.; Liu, J.; Wang, Y.; Lin, Y. *J. Mater. Chem.* **2009**, *19*, 46−59.
(42) Nakada, M.; Ishihara, A.; Mitsushima, S.; Kamiya, N.; Ota, K. *Electrochem. Solid St.* **2007**, *10*, F1−F4.

DOI: 10.1021/cs501429g
ACS Catal. 2015, 5, 2242−2249

(43) Liao, S.; Holmes, K.-A.; Tsaprailis, H.; Birss, V. I. *J. Am. Chem. Soc.* **2006**, *128*, 3504−3505.
(44) Burton, B. B.; Kang, S. W.; Rhee, S. W.; George, S. M. *J. Phys. Chem. C* **2009**, *113*, 8249−8257.
(45) Van Tran, T.; Turrell, S.; Eddafi, M.; Capoen, B.; Bouazaoui, M.; Roussel, P.; Berneschi, S.; Righini, G.; Ferrari, M.; Bhaktha, S. N. B.; Cristini, O.; Kinowski, C. *J. Mol. Struct.* **2010**, *976*, 314−319.
(46) Li, G. C.; Pickup, P. G. *J. Power Sources* **2007**, *173*, 121−129.
(47) Crabb, E. M.; Marshall, R.; Thompsett, D. *J. Electrochem. Soc.* **2000**, *147*, 4440−4447.
(48) Nakanishi, H.; Nishimoto, T.; Nakamura, R.; Yotsumoto, A.; Yoshida, T.; Shoji, S. *Sens. Actuators* **2000**, *79*, 237−234.
(49) Dougherty, R. C. *J. Chem. Phys.* **1998**, *109*, 7372−7378.
(50) Li, C.-J.; Yang, G.-J.; Li, C.-X. *J. Therm. Spray Technol.* **2012**, *22*, 192−206.
(51) Liu, Y.; Mustain, W. E. *J. Am. Chem. Soc.* **2013**, *135*, 530−533.
(52) Park, H.-Y.; Jeon, T.-Y.; Jang, J. H.; Yoo, S. J.; Choi, K.-H.; Jung, N.; Chung, Y.-H.; Ahn, M.; Cho, Y.-H.; Lee, K.-S.; Sung, Y.-E. *Appl. Catal. B: Environ.* **2013**, *129*, 375−381.
(53) Chen, S.; Wei, Z.; Qi, X.; Dong, L.; Guo, Y. G.; Wan, L.; Shao, Z.; Li, L. *J. Am. Chem. Soc.* **2012**, *134*, 13252−13255.
(54) Willsau, J.; Heitbaum, J. *J. Electroanal. Chem.* **1984**, *161*, 93−101.

DOI: 10.1021/cs501429g
ACS Catal. 2015, 5, 2242−2249